Nanoscale Advances

ROYAL SOCIETY OF CHEMISTRY

PAPER

View Article Online
View Journal | View Issue

Cite this: *Nanoscale Adv.*, 2020, **2**, 1551

Clearance of single-wall carbon nanotubes from the mouse lung: a quantitative evaluation†

Minfang Zhang, *[a] Ying Xu,[a] Mei Yang,[a] Masako Yudasaka[bc] and Toshiya Okazaki [a]

Based on the characteristics of carbon nanotubes (CNTs) that absorb light in the near-infrared region, we have developed a method to quantify the biodistribution of CNTs in mouse tissues such as the liver, lungs and spleen. By using this method, the kinetic biodistribution of single-walled CNTs (SWNTs) after intravenous injection into mice for 60 days has been successfully investigated. The results show that the biodistribution of CNTs was diameter-dependent by comparing two different diameters of SWNTs. The SWNTs with larger diameters (1–5 nm) accumulated more in the liver or spleen but less in the lungs than those with smaller diameters (0.7–0.9 nm). The quantities of both SWNTs in the liver and lungs decreased with time and showed no significant change in the spleen, which is also confirmed by histological analysis. In particular, the results have demonstrated that both SWNTs are cleared from the lungs almost completely within 60 days, suggesting that the pulmonary toxicity of SWNTs would be low when low amounts of CNTs (<70 μg g^{-1} of tissue) enter inside the lungs. In addition, no obvious inflammatory responses are found from the measurement of the cytokines TGF-β1, IL-6, INF-γ, and TNF-α in the plasma and organs after the injection of both SWNTs into mice.

Received 15th January 2020
Accepted 4th March 2020

DOI: 10.1039/d0na00040j

rsc.li/nanoscale-advances

1. Introduction

Carbon nanotubes (CNTs)[1] are cylindrical molecules that consist of rolled-up sheets of single-layer or multi-layer carbon atoms. They are classified into single-walled CNTs (SWNTs)[2] and multi-walled CNTs (MWNTs).[1] Due to their unique physical and chemical properties, CNTs have been developed for applications in many fields, including electronic engineering, energy storage, machinery, and even nanomedicine.[3–8] With the widespread development and use of CNTs, there are increasing opportunities for individuals to be exposed to CNTs.[9] Because CNTs have a fiber-like shape, similar to that of asbestos, there is increasing public concern that respiratory exposure to CNTs might increase the risk of lung cancer.[10–12] Moreover, the stable graphite structure of CNTs makes them resistant to biodegradation, increasing concerns about their long-term safety. According to the International Agency for Research on Cancer (IARC, 2002), lung fibrosis and thoracic tumors are often observed when fiber clearance from the lungs is slow. CNTs were shown to persist in the lungs for 90 days or 364 days after intratracheal instillation in rats.[13–15] CNTs implanted in rats also persisted in the subcutaneous tissues for 2 years without degradation.[16]

However, recent studies showed that CNTs can be biodegraded by enzymes such as horseradish peroxidase[17,18] and myeloperoxidase (MPO),[19] macrophages[20,21] and neutrophils.[22] Several studies on the biodegradation of CNTs *in vivo* have also been performed. Nunes *et al.* stereotactically injected amine-functionalized MWNTs into the cortex of the mouse brain[23] and found that MWNTs were predominantly internalized within microglia, the resident macrophages of the brain, at early time points. Transmission electron microscopy (TEM) analysis of the tissue sections revealed severe nanotube structural deformities, reduced length, and loss of the cylindrical structure, suggesting that CNT degradation begins within 2 days post-injection. Elgrabli *et al.* intratracheally instilled CNTs into rat lungs and found a significant decrease in the CNT length 15 days after instillation, suggesting that CNTs are cleaved in the rat lung.[24] Kagan's group demonstrated that SWNTs might be degraded in lung macrophages *via* an oxide-dependent process.[25] However, few studies have addressed the biodegradation of CNTs in animal tissues, and no quantitative analysis has been performed due the lack of appropriate methodologies for evaluating the long-term biodistribution of CNTs in animal organs.

So far, CNTs have been detected in biological environments using radioactive elements or fluorescent labels,[26,27] but these labels may dissociate from CNTs or decay and lose activity over time. Similarly, carbon nanomaterials can be labeled with metal

[a]*CNT Application Research Center, National Institute of Advanced Science and Technology, Higashi, Tsukuba, Ibaraki, 305-8565, Japan. E-mail: m-zhang@aist.go.jp*
[b]*Research Institute of Nanomaterials, National Institute of Advanced Science and Technology, 1-1-1 Higashi, Tsukuba, Ibaraki, 305-8565, Japan*
[c]*Faculty of Science & Technology, Meijo University, 1-501 Shiogamaguchi, Tenpaku-ku, Nagoya 468-8502, Japan*

† Electronic supplementary information (ESI) available. See DOI: 10.1039/d0na00040j

nanoparticles,[28] and intrinsic metal impurities such as iron[29] or nickel[24] within raw CNTs have also been used to estimate the persistence of CNTs by magnetic resonance imaging or inductively coupled plasma atomic emission spectroscopy (ICP-AES).[28,30] However, the low metal content limits the accuracy of measurements obtained with this method, which may only be suitable for use with a few types of CNTs.

To overcome the problems associated with indirect detection of CNTs, studies relying on their intrinsic physical properties, such as Raman spectroscopy[31–33] or fluorescence imaging,[34,35] have also been performed. However, these methods are only suitable for use with SWNTs and are not suitable for long-term studies because SWNTs aggregate, decreasing the intensity of the signal. On the other hand, optical absorption is generally used for quantification of materials in solution. The concentration of CNTs in various dispersions can be easily determined by measurement of the optical absorbance, based on the Beer–Lambert law. Specifically, CNTs absorb light in the near-infrared (NIR) region, a range of wavelengths in which components of cells and tissues, such as protein and water, have almost no absorption.[36] We have successfully used NIR absorption to measure the cellular uptake of CNTs with less interference from bio-components.[36] This method is useful for all types of nanocarbons, including SWNTs, MWNTs, and other carbon nanomaterials such as carbon nanohorns (CNHs).[37,38] In this study, we used this approach to study the biodistribution of CNTs *in vivo*. We quantitatively measured the concentration of CNTs in the liver, lungs, and spleen of mice over a period of 60 days after intravenous administration of two commonly used types of SWNTs with larger or smaller diameters. SWNTs with both diameters were cleared from the lungs almost completely within 60 days. In addition, the biodistribution of CNTs was diameter-dependent. The smaller-diameter SWNTs (Sd-CNTs) accumulated more in the lungs than in the spleen, while the larger-diameter SWNTs (Ld-CNTs) preferentially accumulated in the spleen rather than the lungs. The low toxicity of SWNTs was also confirmed by measuring the levels of cytokines, namely TGF-β1, IL-6, INF-γ, and TNF-α, in plasma and tissue lysates. These results suggest that the risk of pulmonary toxicity of SWNTs would be low if a low amount of SWNTs entered inside the lungs.

2. Results

2.1 Characteristics of CNTs

The characteristics of the two types of SWNTs with larger diameters (Ld-CNTs) and smaller diameters (Sd-CNTs) provided by the manufacturers are listed in Table 1. The diameters of Ld-CNTs and Sd-CNTs were approximately 1–5 nm and 0.7–0.9 nm, respectively, which were roughly consistent with the measurements obtained from TEM images (Fig. 1a and b). The combustion temperatures were approximately 570 °C and 400 °C, measured by using a thermal gravimetric analyzer (TGA) (Fig. SI-1a†), and the residual weights at 1000 °C were approximately 0% and 2% for Ld-CNTs and Sd-CNTs, respectively.

The Ld-CNTs or Sd-CNTs were homogeneously dispersed in an aqueous bovine serum albumin (BSA) solution and did not precipitate over a period of 3 months. The Ld-CNTs and Sd-CNTs in aqueous dispersions were greater than 1 μm in length (Fig. 1c and d). Dynamic light scattering (DLS) measurements showed that the particle size distributions of Ld-CNTs and Sd-CNTs in dispersions were 70–100 nm and 300–420 nm, respectively, and no macro-sized particles were found (Fig. SI-1b†).

2.2 Quantitative analysis of CNTs in the lungs, liver, and spleen

2.2.1 NIR light absorption method. Our NIR light absorption measurement method consists of three steps: preparation of calibration lines, preparation of tissue lysates, and measurement of optical absorbance. The most important step is

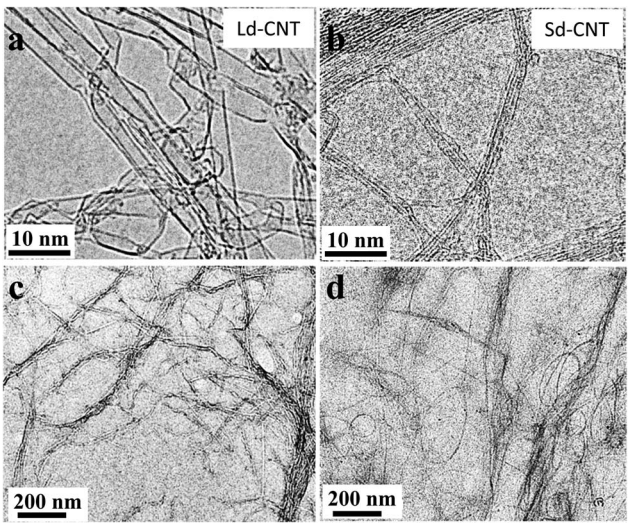

Fig. 1 Characteristics of large-diameter carbon nanotubes (Ld-CNTs) and small-diameter carbon nanotubes (Sd-CNTs). Transmission electron microscopy (TEM) images of Ld-CNTs (a), Sd-CNTs (b), and dispersions of Ld-CNTs (c) and Sd-CNTs (d) in BSA.

Table 1 Characteristics of Ld-CNTs and Sd-CNTs

	Pristine CNTs (catalogue data)				CNT/BSA dispersion	
Name in this study	Trade name	Raman (G/D)	Diameter (nm)	Metals (wt%)	DLS (nm)	Length (μm)
Ld-CNTs	SG-CNTs	1.5–5.7	1–5	<2%	80	>1 μm
Sd-CNTs	CoMoCat SWNTs	>10	0.7–0.9	<5%	350	>1 μm

the preparation of tissue lysates because the tissue needs to be dissolved completely to avoid the effects of light scattered from any undissolved biomaterials. The tissue lysates obtained in this study were transparent, as shown in Fig. SI-2a,† and the absorbance at 750 nm of tissue lysates prepared from the liver, lungs, and spleen of the control mice (without injection) was less than 0.01 (Fig. SI-2b, and c†). This indicated not only that the tissue was almost completely dissolved, but also that the lower detection limit of CNTs was less than 0.025 μg mL^{-1} in the liver lysate and 0.01 μg mL^{-1} in the lung lysate. The validity of these measurements was confirmed using mimic samples that were prepared by mixing the Ld-CNT powder with crushed liver and then performing the lysing process (Fig. SI-2d†). These lysates were transparent, and the absorbance at 750 nm of Ld-CNT-containing lysates with three different, known concentrations of CNTs resulted in the correct concentration based on the calibration line (Fig. SI-2c,† red circle), indicating the high reliability of this method.

2.2.2 Quantitative analysis of CNTs in tissues by NIR light absorption. The concentration of CNTs in the liver, lungs, and spleen of the mice after intravenous injection of Ld-CNTs or Sd-CNTs was estimated from the absorbance of the tissue lysates at 750 nm using calibration curves (Fig. SI-3a and b†). The results are shown in Fig. 2. More Ld-CNTs than Sd-CNTs accumulated in the liver and spleen (Fig. 2a, c), but in the lungs, accumulation of Sd-CNTs was higher than that of Ld-CNTs (Fig. 2b). The concentrations of Ld-CNTs and Sd-CNTs in the liver and lung lysates decreased with time. The amounts of Ld-CNTs and Sd-CNTs in the spleens of individual animals varied widely, which prevents accurate analysis of the time-course of accumulation (Fig. 2c). Notably, the amount of Ld-CNTs and Sd-CNTs in the lungs (Fig. 2b) from about 0.8 and 3.5% of the injected dose (about 15 μg g^{-1} and 70 μg g^{-1} of tissue, respectively) decreased to almost zero by day 60 (D60). For both Ld-CNTs and Sd-CNTs, the total amounts in the liver, spleen, and lungs decreased by about 15% of the injected dose from D1 to D60 (Fig. 2d).

2.2.3 Histological analysis of CNTs in tissues. The livers became dark in appearance after the injection of Ld-CNTs and Sd-CNTs (Fig. 3a and b, insets). Typical optical microscopy images of nuclear fast red solution (kernechtrot)-stained tissue sections (Fig. SI-4†) or unstained sections (Fig. 3a and b) showed that the agglomerated CNTs in the liver appeared as black spots and that the size of these deposits increased with time. Agglomerates of Ld-CNTs and Sd-CNTs were found in the hepatic sinusoids (Fig. SI-4†), where they were likely taken up by Kupffer cells, in agreement with the results of a previous ultrastructural localization study on CNHs.[28] The amount of CNTs in the liver was estimated by measuring the areas of these black spots with image analysis software, as reported by us previously.[39] The black areas representing agglomerates of Ld-CNTs or Sd-CNTs decreased by about 50% from D1 to D30, with no further decrease from D30 to D60 (Fig. 3c and d).

The color of the lungs of the Ld-CNT-injected mice (Fig. 4a, inset picture) did not appear different from that of the control mice (not shown), while the lungs became slightly dark after Sd-

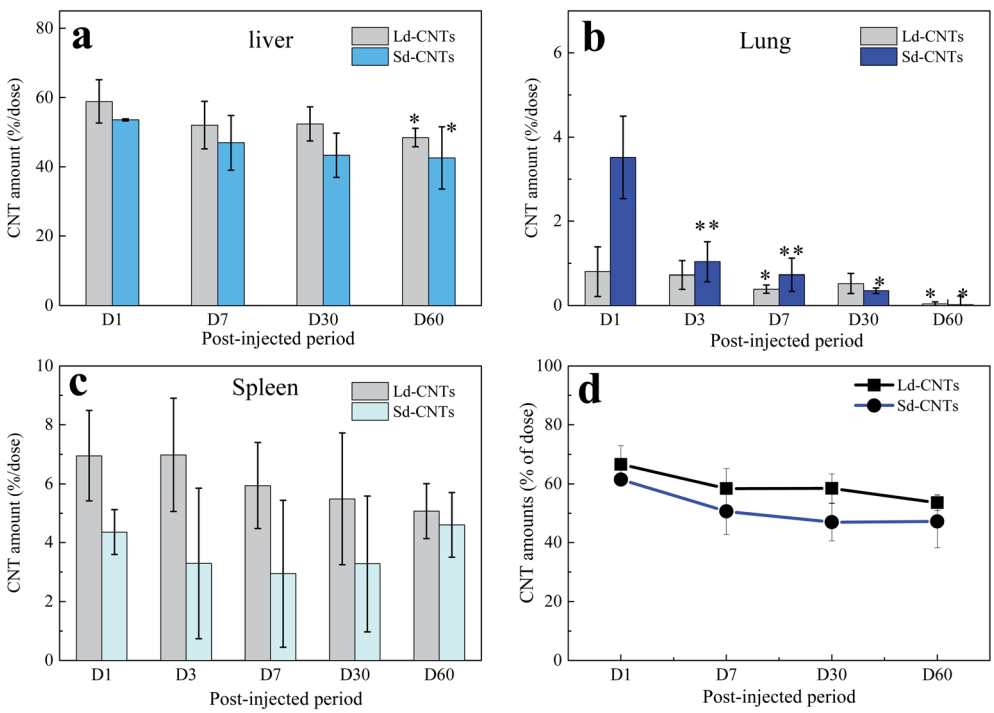

Fig. 2 Changes in the amounts of carbon nanotubes (CNTs) in the liver (a), lungs (b), and spleen (c), and the total amount in the liver, lungs, and spleen (d) after a single intravenous dose of large-diameter or small-diameter CNTs (Ld-CNTs and Sd-CNTs, respectively) from day 1 to day 60 post-injection. The amounts of CNTs in each organ were calculated by measuring the absorbance of tissue lysates at 750 nm. All data are shown as a percentage of the total injected dose [mean ± standard deviation (SD), $n = 5$]. $^{**}P<0.01$ and $^{*}P<0.05$ *vs.* the values on day 1.

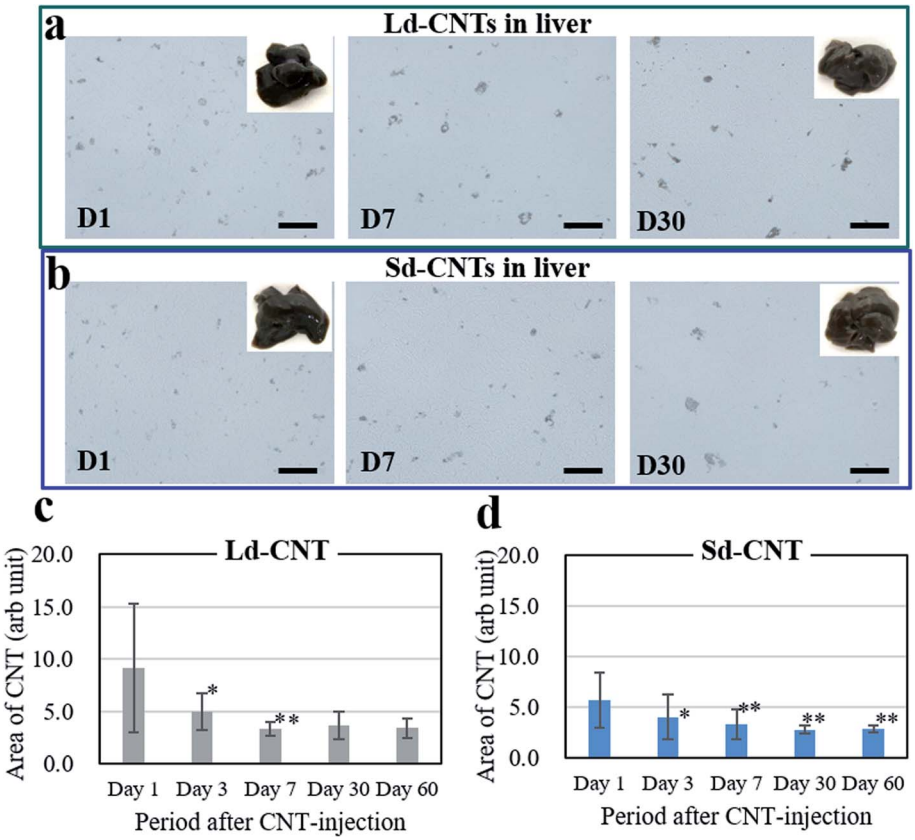

Fig. 3 Optical microscopy images of unstained mouse livers harvested on days 1, 7, and 30 after a single intravenous dose of large-diameter carbon nanotubes (Ld-CNTs) (a) or small-diameter carbon nanotubes (Sd-CNTs) (b). Images of mouse livers after intravenous injection of Ld- and Sd-CNTs are shown in the insets in (a) and (b), respectively. The average areas of the black spots representing Ld-CNTs (c) or Sd-CNTs (d) in 20 images per tissue sample. Scale bar: 50 μm. $^{**}P<0.01$ and $^{*}P<0.05$ *vs.* the values on day 1.

CNT injection (Fig. 4b, inset). The area of the black spots representing Sd-CNTs in the lung sections clearly decreased from D1 to D7 (Fig. 4b and e), while on D30, there was no difference between the Sd-CNT and Ld-CNT-injected mice (Fig. 4) or control mice. These results were consistent with the quantification results obtained using the NIR light absorption method (Fig. 2). The Sd-CNTs seemed to accumulate in the alveolar macrophages (Fig. SI-5†).

The spleens also became dark after injection of Ld-CNTs or Sd-CNTs. The areas of the dark spots in the tissue sections from the mice injected with Ld-CNTs and Sd-CNTs were similar and increased with time (Fig. SI-6 and SI-7†). These results did not coincide with those obtained from the NIR light absorption method (Fig. 2). This might be due to the increased agglomeration of CNTs over time, causing them to be more visible at later time points. Here, the accumulation of Ld-CNTs was greater than that of Sd-CNTs, which was determined by the NIR light absorption method, and the accumulation of Ld-CNTs and Sd-CNTs in the spleen did not decrease over time.

2.3 Toxicity assessment

The levels of the pro-inflammatory cytokines TGF-β, IL-6, IFN-γ, and TNF-α in plasma and tissue lysates were measured to evaluate possible inflammatory reactions caused by Ld-CNTs and Sd-CNTs. The cytokine levels in the mice after receiving CNTs longer than 3 days were similar to those of the control group and no significant differences between groups were found (Fig. 5a–d; SI-8 and SI-9†). It is also found that the Ld-CNT injected groups exhibited higher levels of the cytokines TGF-β1 and TNF-α in the plasma (Fig. 5) and IL-6 in the liver lysates (Fig. SI-9†) at the early time-points of day 1 or day 3 compared with control groups. These results indicated that CNTs would activate macrophages and secrete pro-inflammatory cytokines after injection at early time points.

In addition, despite the apparent accumulation of CNTs, histological observation revealed normal levels of inflammatory responses, such as apoptosis, necrosis, cellular degeneration, and neutrophil infiltration in the liver, lungs, and spleen. A visual inspection of the organs did not indicate any signs of weakness or illness. The body weights of the control mice and the CNT-injected mice were equivalent (Fig. SI-10†).

3. Discussion

3.1 NIR light absorption for evaluation of CNTs in organs

In this study, we report a method of directly using the characteristics of CNTs, which absorb light in the NIR region, to estimate the concentration of CNTs in the liver, spleen, and lungs over a relatively long period of time, about 60 days. This

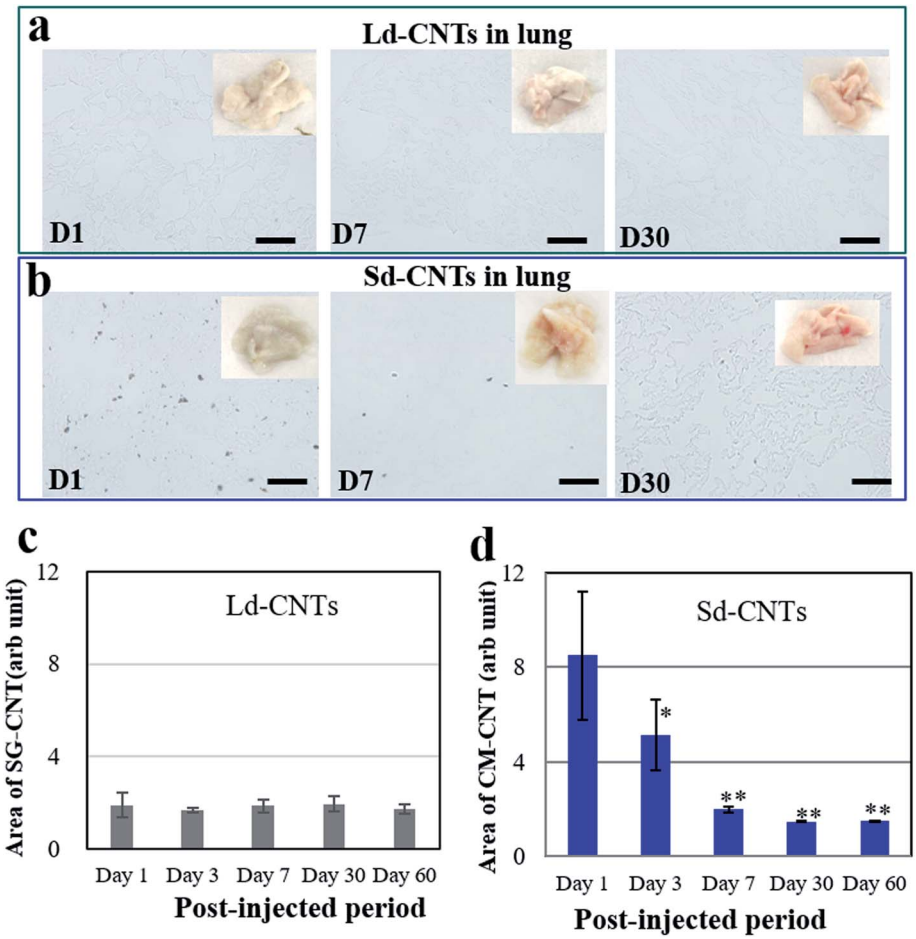

Fig. 4 Optical microscopy images of unstained mouse lung tissues harvested on days 1, 7, and 30 after a single intravenous dose of large-diameter carbon nanotubes (Ld-CNTs) (a) or small-diameter carbon nanotubes (Sd-CNTs) (b). Photographs of mouse livers after intravenous injection of Ld-CNTs and Sd-CNTs are shown in the insets in (a) and (b), respectively. The average areas of the black spots representing Ld-CNTs (c) or Sd-CNTs (d) in 20 images per tissue sample. Scale bar: 50 μm. $^{**}P<0.01$ and $^{*}P<0.05$ *vs.* the values on day 1.

method showed high accuracy, as confirmed by the accurate measurement of known concentrations of CNTs (Fig. SI-1†). To further confirm the measurement accuracy, we performed an *in vivo* study using CNHs with Gd labels encapsulated inside the horns (Gd@CNHs),[30] where CNHs have optical absorption properties similar to those of CNTs and the labels could be used to estimate the quantities of CNHs in tissues by measuring the Gd content.[30] The amount of CNHs in the liver 1 day and 30 days after intravenous injection of Gd@CNHs into mice was estimated using two methods, the NIR absorbance method described in this study and a method using ICP-AES to measure the Gd content, as reported by us previously.[30] The amounts of Gd@CNHs in the liver estimated using the two methods were similar (Fig. SI-11†), indicating the accuracy of the method used in this study. In addition, the absorbance of the control samples at 750 nm (*e.g.*, liver; Fig. SI-2b†) indicated that the lower limit of detection of the NIR absorbance method is less than 0.025 μg mL^{-1}, which is much more sensitive than that of methods using metal labels (limit of detection >0.1 μg mL^{-1}).[24]

It is also found that the relative errors for results obtained from the spleens (Fig. 2c) were higher than those from the livers and lungs. We believed that the measurement error was mainly from the different weights of the spleen for different mice, which were in the range of 0.06–0.12 g. For decreasing the relative errors, it would be better to use larger numbers of mice more than 6 for each group in future studies.

3.2 Diameter-dependent biodistribution

The data acquired using the NIR light absorption method indicate that the accumulation of Ld-CNTs in the liver, lungs, and spleen is different from that of Sd-CNTs. The size-dependent biodistribution of CNTs has been studied with CNTs of different lengths (short or long).[40] Short nanotubes with appropriately functionalized surfaces have a long retention time in the blood and can be partly excreted in the urine and feces,[31,41] indicating that CNTs with short lengths might show improved accumulation in all organs of the body. Our previous histological study showed that small CNHs (30–50 nm) accumulated in the liver and spleen more slowly than large CNHs (100 nm).[39] However, no information has been reported on the difference in distribution of CNTs with similar long lengths (>1 μm) but different diameters.

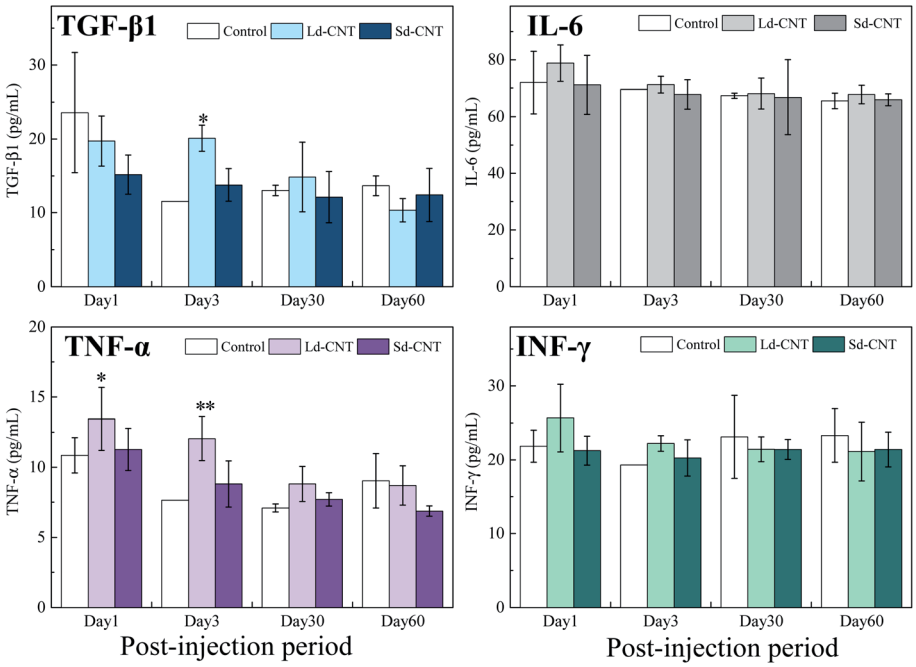

Fig. 5 Concentrations of TGF-β1, IL-6, TNF-α, and INF-γ in the plasma of mice 1, 3, 30, and 60 days after injection of large-diameter carbon nanotubes (Ld-CNTs) or small-diameter carbon nanotubes (Sd-CNTs). Data are expressed as the mean ± SD ($n = 5$). **P<0.01, *P<0.05 *vs.* the values of the control.

Sd-CNTs accumulated less in the liver and spleen (Fig. 2a and c) but a little more in the lungs (Fig. 2b) than Ld-CNTs at a post-injection period of 24 hours. This might be because the uptake of small-diameter CNTs by macrophages is lower than that of larger-diameter CNTs, as reported by us previously.[36] Sd-CNTs might therefore be retained longer in the vasculature, resulting in greater accumulation in the lungs, than CNTs with larger diameters. The details remain to be clarified in future work.

3.3 Clearance of CNTs from the lungs

Another important finding of this study is the clearance of CNTs from the lungs. By both histological observations and quantitative measurement of the CNT concentration using NIR absorption, both Ld-CNTs and Sd-CNTs were almost completely cleared from the lungs by the 60th day after intravenous injection. Together with the results showing the low toxicity of the CNTs (Section 3.4), a small amount of CNTs in the human lung (<70 μg g^{-1} of tissue) is unlikely to present a strong safety risk. This information may be significant for the industrial application of CNTs under appropriate safety management.

Some previous studies have shown that CNTs persisted in the lungs of rats for up to 90 days or 364 days after intratracheal instillation of SWCNTs[13] or MWCNTs.[14] However, Elgrabli *et al.* studied the persistence and clearance of CNTs after respiratory administration.[24] They found that the CNTs did not significantly cross the pulmonary barrier but presented in the lungs 6 months after a unique instillation and could be eliminated from the lungs by macrophages. Kagan's group instilled oxidized SWNTs into the lungs of MPO knockout[42] or nicotinamide adenine dinucleotide phosphate (NADPH) oxidase-deficient mice *via* pharyngeal aspiration[25] and found that the clearance of SWNTs was markedly impaired in both mutants compared with wild-type mice, indicating the possible biodegradation of SWNTs in the lungs *via* enzymatic oxidation in macrophages. In this study, Sd-CNTs seemed to accumulate in the alveolar macrophages (Fig. SI-5†). Therefore, the clearance of Ld-CNTs and Sd-CNTs from the lungs in this study was probably also due to their degradation by macrophages, as demonstrated by Elgrabli *et al.* and Kagan *et al.*[24,25,43] This study and the previous studies differ in the degree of degradation, whether near-complete removal of CNTs (Fig. 2 and 4) or partial removal of CNTs.[24] This difference could be due to the circulation of CNTs in the blood after intravenous injection, which result in a lower concentration of CNTs in the lung and therefore more rapid and complete clearance of CNTs by macrophages. For intratracheal instillation, CNTs were directly injected into the lungs and engulfed slowly by alveolar macrophages.[24] A lot of CNTs existed outside the macrophages that were impossible to degrade. On the other hand, the intratracheal instillation resulted in a high concentration of CNTs in the lungs, which might induce macrophage dysfunction,[44,45] reducing the CNT clearance, as described by Shinohara *et al.*[14]

In addition, it is also impossible to rule out the possibility that a small number of CNTs remaining in the vessel lumen could travel to other organs *via* the vascular system, resulting in clearance from the lungs. To clarify the possibility of any transference of CNTs from the lungs to other organs or excretion, the measurement of the CNT amount in the whole mouse body would be needed in a future study, as reported in our previous study.[30]

4. Conclusion

In this study, we developed a quantification method using NIR light absorption to estimate the biodistribution of CNTs in organs after intravenous injection into mice. The advantages of this method are its higher sensitivity than that of previous methods of quantification and its wide applicability for all kinds of CNTs. By using NIR light absorption measurements and histological analysis, we show the biodistribution of SWNTs with two different diameters in the liver, spleen, and lungs over time. The accumulation of Ld-CNTs in the lungs was less than that of Sd-CNTs, while the accumulation of Ld-CNTs in the liver and spleen was greater than that of Sd-CNTs, suggesting that the biodistribution of SWCNTs is diameter-dependent. Moreover, the concentration of both Ld-CNTs and Sd-CNTs in the liver decreased to about 10% of the injected dose in 60 days after intravenous administration, while the CNTs were almost completely cleared from the lungs by this time. The clearance of SWNTs from the lungs could be due to degradation in macrophages or movement to other sites *via* the vasculature. Both Sd-CNTs and Ld-CNTs were non-toxic, based on the measurement of cytokines in the plasma and tissue.

5. Experimental section

5.1 CNT dispersions

Two types of SWNTs were used in this study. SWNTs produced by the super-growth method (SG-CNTs; Zeon Nanotechnology Co., Tokyo, Japan) have a large diameter of 1–5 nm (referred to as Ld-CNTs). SWNTs produced by the CoMoCAT synthesis process (SG65i; Sigma-Aldrich, St. Louis, MO, USA) have a small diameter of 0.7–0.9 nm (Sd-CNTs). Ld-CNTs or Sd-CNTs were dispersed in aqueous solutions of bovine serum albumin (BSA) (Nacalai Tesque, Kyoto, Japan). Dispersion was achieved by a standard process.[46,47] Briefly, CNTs (about 70 mg) were dispersed in 50 mL of an aqueous solution of 10 mg mL^{-1} BSA by treatment for 5 h in an ultrasonic homogenizer (VC-750; Sonics & Materials, Newtown, CT, USA). After sonication, the CNT dispersions were centrifuged at 3000×*g* for 1 h and filtered through a cell strainer with 40 μm nylon mesh (Becton Dickinson, Franklin Lakes, NJ, USA). The resulting homogeneous dispersion of CNTs was maintained as a stock at 2–4 °C. The concentration of Ld-CNTs or Sd-CNTs in BSA solution was approximately 1 mg mL^{-1}, and the dispersions were adjusted in a solution of phosphate-buffered saline (PBS).

5.2 Characterization of CNT dispersions

The morphologies of the Ld-CNTs, the Sd-CNTs, and the dispersions were observed by high-resolution TEM (Topcon 002B; Topcon, Tokyo, Japan) at an acceleration voltage of 120 kV. For TEM observation of CNT dispersions, one drop of the dispersion was placed on a TEM grid with a carbon film coating. The particle sizes of the CNTs in dispersions were also estimated by dynamic light scattering (DLS) (FPAR-1000; Otsuka Electronics, Osaka, Japan). The metal content of pristine CNTs was measured in oxygen gas using a thermal gravimetric analyzer (TGA) (TA Instruments, New Castle, DE, USA) heated from room temperature to 1000 °C at a rate of 10 °C min^{-1}.

5.3 *In vivo* studies

5.3.1 Study design. All animal studies were performed in accordance with the Guidelines for Proper Conduct of Animal Experiments (Japan) and approved by the Animal Care and Use Committee of the National Institute of Advanced Industrial Science and Technology, Japan.

Eighty female BALB/cAJcl mice, aged 6 weeks, were purchased from CLEA Japan (Tokyo). All animals were acclimatized in a pathogen-free animal facility for 1 week before CNT injection. The animals were divided into three groups: control (PBS), Ld-CNTs, and Sd-CNTs. A 200 μL injection of the PBS or CNT dispersion in PBS was administered *via* the tail vein. Because the concentration of the CNTs in the dispersion was approximately 1 mg mL^{-1}, each mouse received a CNT dose of approximately 10 mg kg^{-1}. At each of the five time points (days 1, 3, 7, 30, and 60), mice were anesthetized with isoflurane and sacrificed by blood collection (1 mL) from the abdominal aorta. The tissues were washed by perfusion of a washing solution through the portal vein of the liver. The washing solution consisted of Hank's buffered saline solution (HBSS; Fujifilm Wako, Tokyo, Japan) containing 0.5 mM *O*,*O*′-bis(2-aminoethyl)ethyleneglycol-*N*,*N*,*N*′,*N*′-tetraacetic acid (EGTA; Dojindo Molecular Technologies, Kumamoto, Japan) and 10 mM 4-(2-hydroxyethyl)-1-piperazineethanesulfonic acid (HEPES; Sigma-Aldrich). After the tissue was perfused, the liver, spleen, and lungs were removed and weighed. A portion of each organ was fixed in 10% neutral-buffered formalin. The remaining tissues were cut into small pieces with scissors and transferred into sterile bottles for preparation of tissue lysates.

5.3.2 Tissue lysate preparation. To prepare liver lysates, liver pieces from each mouse were dispersed in 10 mL of HBSS containing 0.05% collagenase type I (Fujifilm Wako) and 10 mM HEPES. After incubation at 37 °C for 1 hour, the liver dispersion was mixed with sodium dodecylbenzenesulfonate (SDBS; Tokyo Chemical Industry Co., Tokyo, Japan) (10 mL of a 10 mg mL^{-1} solution) and incubated at 37 °C overnight. After removing 0.5 mL for cytokine analysis, the remaining solution was heat-treated in an 80 °C water bath for 2 hours. To prepare lysates of the spleen and lungs, the tissues were dispersed in 2 mL of a tissue solubilizer solution (Solvable; PerkinElmer, Waltham, MA, USA) and then incubated at 37 °C overnight. Then, 0.2 mL of the solution was removed for cytokine analysis, and the remaining solution was used for CNT quantification.

5.3.3 Quantitative estimation of CNTs in organs. The amount of CNTs in each tissue (liver, lungs, and spleen) was estimated by NIR optical absorption. First, calibration curves for Ld-CNTs and Sd-CNTs in BSA were prepared by measuring the absorbance of CNT dispersions at various concentrations (0–100 μg mL^{-1}) at a wavelength of 750 nm. Then, the absorbance of the tissue lysates was measured at 750 nm and the concentration of CNTs in each tissue sample was estimated based on the calibration curve, as described previously.[36] The amount of CNTs in the tissue relative to the injected dose (%ID) was calculated by using the following equation:

$$\%\mathrm{ID} = \{[\mathrm{CNTs}]\ \mathrm{tissue} \times \mathrm{Vtissue}\}/\{[\mathrm{CNTs}]\mathrm{injected} \times \mathrm{Vinjected}\}$$

in which [CNTs]tissue: concentration of CNTs in the tissue lysates; Vtissue: volume of the tissue lysate (Vliver = 20 mL, Vlung or Vspleen = 2 mL); [CNTs]injected: concentration of CNTs in the injected CNT dispersion (1 mg mL^{-1}); Vinjected: volume of the injected CNT dispersion (0.2 mL).

5.3.4 Histological studies. Liver, spleen, and lung tissues fixed in 10% neutral-buffered formalin were embedded in paraffin and cut into 4 μm thick sections. Sections were stained with nuclear fast red solution (kernechtrot) (Sigma-Aldrich) or left unstained and analyzed under an optical microscope (BX 60; Olympus, Tokyo, Japan). The amount of Ld-CNTs and Sd-CNTs in each tissue type was estimated by measuring the total area of the black spots in 20 images taken at 50× magnification using Winroof image analysis software (Mitani Visual, Fukui, Japan).

5.3.5 Cytokine measurements. Concentrations of the cytokines TGF-β1, IL-6, IFN-γ, and TNF-α in plasma and tissue lysates were measured using mouse enzyme-linked immunosorbent assay (ELISA) kits purchased from R&D Systems (Minneapolis, MN, USA), according to the manufacturer's protocols. Plasma was obtained by centrifuging the blood at 100×*g* for 15 min.

Author contributions

Minfang Zhang conceived and designed the experiments. Ying Xu and Minfang Zhang performed the animal experiments. Mei Yang prepared the samples. Minfang Zhang, Masako Yudasaka, and Toshiya Okazaki analysed the data. Minfang Zhang wrote the manuscript. All the authors discussed the results and commented on the manuscript.

Conflicts of interest

There are no conflicts to declare.

Acknowledgements

This work was supported partly by the Japan Society for the Promotion of Science (JSPS) (KAKENHI Grant-in-Aid for Scientific Research B, 17H02742) and by the ZEON Corporation.

References

1 S. Iijima, *Nature*, 1991, **354**, 56.
2 S. Iijima and T. Ichihashi, *Nature*, 1993, **363**, 603.
3 M. F. De Volder, S. H. Tawfick, R. H. Baughman and A. John Hart, *Science*, 2013, **339**, 535.
4 R. H. Baughman, A. A. Zakhidov and W. A. de Heer, *Science*, 2002, **297**, 787.
5 C. W. Tan, K. H. Tan, Y. T. Ong, A. R. Mohamed, S. H. S. Zein and S. H. Tan, *Environ. Chem. Lett.*, 2012, **10**, 265.
6 Z. Liu, S. Tabakman, K. Welsher and H. Dai, *Nano Res.*, 2009, **2**, 85.
7 M. Martincic and G. Tobias, *Expert Opin. Drug Delivery*, 2015, **12**, 563.
8 I. M. Feigel, H. Vedalaa and A. Star, *J. Mater. Chem.*, 2011, **21**, 8940.
9 J. Kolosnjaj-Tabi, J. Just, K. Hartman, Y. Laoudi, S. Boudjemaa, D. Alloyeau, H. Szwarc, L. J. Wilson and F. Moussa, *EBioMedicine*, 2015, **2**, 1697.
10 C. A. Poland, R. Duffin, I. Kinloch, A. Maynard, W. A. H. Wallace, A. Seaton, V. Stone, S. Brown, W. Macnee and K. Donaldson, *Nat. Nanotechnol.*, 2008, **3**, 423.
11 A. Takagi, A. Hirose, T. Nishimura, N. Fukumori, A. Ogata, N. Ohashi, S. Kitajima and J. Kanno, *J. Toxicol. Sci.*, 2008, **33**, 105.
12 A. Takagi, A. Hirose, M. Futakuchi, H. Tsuda and J. Kanno, *Cancer Sci.*, 2012, **103**, 1440.
13 K. Fujita, M. Fukuda, S. Endoh, J. Maru, H. Kato, A. Nakamura, N. Shinohara, K. Uchino and K. Honda, *Toxicol. Lett.*, 2016, **257**, 23.
14 N. Shinohara, T. Nakazato, K. Ohkawa, M. Tamura, N. Kobayashi, Y. Morimoto, T. Oyabu, T. Myojo, M. Shimada, K. Yamamoto, H. Tao, M. Ema, M. Naya and J. Nakanishi, *J. Appl. Toxicol.*, 2016, **36**, 501.
15 J. Pauluhn, *Toxicol. Sci.*, 2010, **113**, 226.
16 Y. Sato, A. Yokoyama, Y. Nodasaka, T. Kohgo, K. Motomiya, H. Matsumoto, E. Nakazawa, T. Numata, M. Zhang, M. Yudasaka, H. Hara, R. Araki, O. Tsukamato, H. Saito, T. Kamino, F. Watari and K. Tohji, *Sci. Rep.*, 2013, **3**, 2516.
17 B. L. Allen, P. D. Kichambare, P. Gou, I. I. Vlasova, A. A. Kapralov, N. Konduru, V. E. Kagan and A. Star, *Nano Lett.*, 2008, **8**, 3899.
18 Y. Zhao, B. L. Allen and A. Star, *J. Phys. Chem. A*, 2011, **115**, 9536.
19 K. Bhattacharya, C. Sacchetti, R. El-Sayed, A. Fornara, G. P. Kotchey, J. A. Gaugler, A. Star, M. Bottini and B. Fadeel, *Nanoscale*, 2014, **6**, 14686.
20 J. Hou, B. Wan, Y. Yang, X. M. Ren, L. H. Guo and J. F. Liu, *Int. J. Mol. Sci.*, 2016, **17**, 409.
21 M. Yang, M. Zhang, M. Yudasaka, S. Iijima and T. Okazaki, *Int. J. Nanomed.*, 2019, **14**, 2797.
22 V. E. Kagan, N. V. Konduru, W. Feng, B. L. Allen, J. Conroy, Y. Volkov, I. I. Vlasova, N. A. Belikova, N. Yanamala, A. Kapralov, Y. Y. Tyurina, J. Shi, E. R. Kisin, A. R. Murray, J. Franks, D. Stolz, P. Gou, J. Klein-Seetharaman, B. Fadeel, A. Star and A. A. Shvedova, *Nat. Nanotechnol.*, 2010, **5**, 354.
23 A. Nunes, C. Bussy, L. Gherardini, M. Meneghetti, M. A. Herrero, A. Bianco, M. Prato, T. Pizzorusso, K. T. Al-Jamal and K. Kostarelos, *Nanomedicine*, 2012, **7**, 1485.
24 D. Elgrabli, M. Floriani, S. Abella-Gallart, L. Meunier, C. Gamez, P. Delalain, F. Rogerieux, J. Boczkowski and G. Lacroix, *Part. Fibre Toxicol.*, 2008, **5**, 20.
25 V. E. Kagan, A. A. Kapralov, C. M. St Croix, S. C. Watkins, E. R. Kisin, G. P. Kotchey, K. Balasubramanian, I. I. Vlasova, J. Yu, K. Kim, W. Seo, R. K. Mallampalli, A. Star and A. A. Shvedova, *ACS Nano*, 2014, **8**, 5610.
26 H. Wang, S. T. Yang, A. Cao and Y. Liu, *Acc. Chem. Res.*, 2013, **46**, 750.
27 N. Dementev, X. Feng and E. Borguet, *Langmuir*, 2009, **25**, 7573.

28 J. Miyawaki, S. Matsumura, R. Yuge, T. Murakami, S. Sato, A. Tomida, T. Tsuruo, T. Ichihashi, T. Fujinami, H. Irie, K. Tsuchida, S. Iijima, K. Shiba and M. Yudasaka, *ACS Nano*, 2009, **3**, 1399.
29 A. Faraj, K. Cieslar, G. Lacroix, S. Gaillard, E. Canet-Soulas and Y. Crémillieux, *Nano Lett.*, 2009, **9**, 1023.
30 M. Zhang, Y. Tahara, M. Yang, X. Zhou, S. Iijima and M. Yudasaka, *Adv. Healthcare Mater.*, 2014, **3**, 239.
31 Z. Liu, C. Davis, W. Cai, L. He, X. Chen and H. Dai, *Proc. Natl. Acad. Sci. U. S. A.*, 2008, **105**, 1410.
32 C. G. Salzmann, B. T. T. Chu, G. Tobias, S. A. Llewellyn and M. L. H. Green, *Carbon*, 2007, **45**, 907.
33 B. D. Holt, K. N. Dahl and M. F. Islam, *Small*, 2011, **7**, 2348.
34 D. A. Heller, S. Baik, T. E. Eurell and M. S. Strano, *Adv. Mater.*, 2005, **17**, 2793.
35 R. Weissleder, *Nat. Biotechnol.*, 2001, **19**, 316.
36 M. Zhang, M. Yang, T. Morimoto, N. Tajima, K. Ichiraku, K. Fujita, S. Iijima, M. Yudasaka and T. Okazaki, *Carbon*, 2018, **127**, 93.
37 M. Zhang, M. Yang, C. Bussy, S. Iijima, K. Kostarelos and M. Yudasaka, *Nanoscale*, 2015, **7**, 2834.
38 M. Zhang, X. Zhou, S. Iijima and M. Yudasaka, Small-sized carbon nanohorns enabling cellular uptake control, *Small*, 2012, **8**, 2524.
39 M. Zhang, T. Yamaguchi, S. Iijima and M. Yudasaka, *Nanomedicine*, 2013, **9**, 657.
40 J. Kolosnjaj-Tabi, K. B. Hartman, S. Boudjemaa, J. S. Ananta, G. Morgant, H. Szwarc, L. J. Wilson and F. Moussa, *ACS Nano*, 2010, **4**, 1481.
41 L. Lacerda, M. A. Herrero, K. Venner, A. Bianco, M. Prato and K. Kostarelos, *Small*, 2008, **4**, 1130.
42 A. A. Shvedova, A. A. Kapralov, W. H. Feng, E. R. Kisin, A. R. Murray, R. R. Mercer, C. M. St Croix, M. A. Lang, S. C. Watkins, N. V. Konduru, B. L. Allen, J. Conroy, G. P. Kotchey, B. M. Mohamed, A. D. Meade, Y. Volkov, A. Star, B. Fadeel and V. E. Kagan, *PLoS One*, 2012, **7**, e30923.
43 D. Elgrabli, W. Dachraoui, C. Ménard-Moyon, X. J. Liu, D. Bégin, S. Bégin-Colin, A. Bianco, F. Gazeau and D. Alloyeau, *ACS Nano*, 2015, **9**, 10113.
44 Y. Tahara, M. Nakamura, M. Yang, M. Zhang, S. Iijima and M. Yudasaka, *Biomaterials*, 2012, **33**, 2762.
45 M. Yang, M. Zhang, Y. Tahara, S. Chechetka, E. Miyako, S. Iijima and M. Yudasaka, *Toxicol. Appl. Pharmacol.*, 2014, **280**, 117.
46 K. Fujita, M. Fukuda, S. Endoh, H. Kato, J. Maru, A. Nakamura, K. Uchino, N. Shinohara, S. Obara, R. Nagano, M. Horie, S. Kinugasa, H. Hashimoto and A. Kishimoto, *Toxicol. Mech. Methods*, 2013, **23**, 598.
47 ISO/TS 19337:2016, Nanotechnologies – Characteristics of Working Suspensions of Nano-objects for in Vitro Assays to Evaluate Inherent Nano-object Toxicity, Technical Committee: ISO/TC 229 Nanotechnologies.